Journal of Computational Physics **171,** 115–131 (2001)
doi:10.1006/jcph.2001.6777, available online at http://www.idealibrary.com on IDEAL®

Streamline Design of Stability Parameters for Advection–Diffusion Problems

Isaac Harari,* Leopold P. Franca,† and Saulo P. Oliveira†,[1]

**Department of Solid Mechanics, Materials, and Systems, Tel Aviv University, 69978 Ramat Aviv, Israel; and †Department of Mathematics, University of Colorado at Denver, Denver, Colorado 80217-3364*
E-mail: harari@eng.tau.ac.il, lfranca@math.cudenver.edu, saulo@math.cudenver.edu

Received June 27, 2000; revised March 12, 2001

The dependence of the computation of advective–diffusive transport phenomena on the orientation of the mesh with respect to the flow direction is analyzed. Poor performance of the classical Galerkin finite-element method in the convection-dominated regime is alleviated by stabilization. We propose definitions of the stability parameter that rationally incorporate the flow direction. Numerical tests compare the performance of the proposed methods with established techniques.

Key Words: advection–diffusion; stabilized method; stability parameter.

CONTENTS

1. INTRODUCTION

The Galerkin finite element method with low-order piecewise polynomials performs poorly for advection-dominated equations. Adding terms to the variational formulation is well-accepted practice, leading to stabilized methods.

In simple settings the standard Galerkin finite-element method produces central difference type approximations. It is well known that the central difference representation of advection terms gives rise to spurious oscillations in advection-dominated regimes. This led to the

[1] Supported by CNPq, Brazil.

0021-9991/01 $35.00

development of upwind difference schemes [17, 18], which are stabilized to preclude oscillations by adding artificial diffusivity. Early upwind finite-element schemes [19], still within the Galerkin framework, were similar. Stability was achieved at the expense of accuracy due to incorrect treatment of diffusion terms, leading to loss of consistency (see, e.g., [14]).

Stabilized finite elements have been around for more than 20 years. These methods have the desirable properties of improving the numerical stability of the Galerkin method and of preserving good accuracy properties. This is achieved by adding terms to the basic Galerkin formulation to retain the weighted residual structure. The streamline upwind/Petrov–Galerkin (SUPG, or streamline diffusion) method was introduced by Hughes and Brooks [5, 15]. Variations of this idea considered for advective–diffusive equations are: the Galerkin/least-squares (GLS) version, introduced by Hughes, Franca, and Hulbert [16], and a few years later, the version termed unusual stabilized finite-element method (USFEM) of Franca *et al.* [6, 9].

The additional terms in stabilized finite elements are residual-based and contain stabilization parameters. The residual-based operators in these terms translate into a streamline diffusion effect. The degree of stabilization in this direction depends on the stabilization parameters. These were originally conceived based on comparisons to exact solutions of one-dimensional test problems on uniform meshes [5]. They were extended to general polynomial discretizations using error estimates [9]. The stabilization parameters were revisited, taking into account a zero-order term in the equation [6, 12]. The parameters are computed explicitly for the Galerkin method enriched with bubbles [7, 10, 11], where the polynomial is piecewise linear enriched with a "residual-free bubble" (RFB) [2, 4]. The residual-free bubble is condensed out yielding a stabilized method with an explicit recipe for the stability parameter.

The design of the stability parameter in previous work ignores the flow direction, or accounts for it in an *ad hoc* fashion (see, e.g., [5]). In this paper we analyze the spurious *anisotropy* inherent in the Galerkin method, i.e., the dependence of the solution on the orientation of the mesh with respect to the flow direction. On the basis of this analysis we propose definitions of the stability parameter that rationally incorporate the flow direction. Numerical tests compare the performance of the proposed method with established techniques.

A family of stabilized methods for advective–diffusive problems, including Galerkin/least-squares, SUPG (also known as streamline diffusion), and the unusual stabilized finite-element method is presented in Section 2. These three methods share the approach of appending to the Galerkin equation terms containing residual-based operators multiplied by stabilization parameters. The analysis of the Galerkin method for the case of a uniform mesh aligned with constant velocity, and the design of stability parameters based on this analysis, are reviewed in Section 3. The presentation is unconventional, suitable for generalization to multi-dimensional configurations, but the results and conclusions are known. In Section 4 more general orientations of the mesh with respect to the flow direction are considered. A simple and economical definition of the stability parameter that rationally accounts for flow direction is proposed. The numerical performance of the proposed method and of established techniques are compared in Section 5.

2. STABILIZED METHODS FOR ADVECTION–DIFFUSION

Let $\Omega \subset \mathbb{R}^d$ be a d-dimensional, open, bounded region with smooth boundary Γ. We partition Ω into nonoverlapping regions (element domains) in the usual way, denoting the union of element interiors $\tilde{\Omega}$, such that $\overline{\Omega} = \overline{\tilde{\Omega}}$.

2.1. *Boundary-Value Problem*

Consider the (homogeneous Dirichlet) advective–diffusive problem of finding a scalar field $u(\mathbf{x})$, such that

$$\mathcal{L}u = f \qquad \text{in } \Omega \text{ and} \tag{1}$$

$$u = 0 \qquad \text{on } \Gamma, \tag{2}$$

where $\mathcal{L}u = -\nabla \cdot (\kappa \nabla u) + \mathbf{a} \cdot \nabla u$, the diffusivity $\kappa(\mathbf{x}) > 0$ is known, $\mathbf{a}(\mathbf{x})$ is the given flow velocity, and $f(\mathbf{x})$ is the prescribed source distribution. Generalization of the results presented herein to problems with other types of boundary conditions is straightforward.

2.2. *Galerkin Approximation*

The Galerkin approximation is stated in terms of the set of functions $\mathcal{V}^h \subset H_0^1(\Omega)$. The standard finite-element method is to find $u^h \in \mathcal{V}^h$ such that

$$a(v^h, u^h) = (v^h, f), \qquad \forall v^h \in \mathcal{V}^h, \tag{3}$$

where $(\cdot, \cdot)$ is the $L_2(\Omega)$ inner product. (The form of the right-hand side assumes sufficiently smooth f.) The bilinear operator is

$$a(v, u) = (\nabla v, \kappa \nabla u) + (v, \mathbf{a} \cdot \nabla u). \tag{4}$$

2.3. *Stabilized Methods*

The standard family of stabilized methods is obtained by appending to the Galerkin equation (3) terms containing residual-based operators multiplied by stabilization parameters τ, namely

$$a(v^h, u^h) + (\bar{\mathcal{L}} v^h, \tau \mathcal{L} u^h)_{\tilde{\Omega}} = (v^h, f) + (\bar{\mathcal{L}} v^h, \tau f)_{\tilde{\Omega}}. \tag{5}$$

Subscripts on inner products denote domains of integration other than Ω. Different stabilized methods are obtained via definitions of the differential operator:

$$\bar{\mathcal{L}} v = \begin{cases} \mathcal{L} v, & \text{GLS [16]} \\ \mathcal{L}_{\text{adv}} v = \mathbf{a} \cdot \nabla v, & \text{SUPG [5]} \\ -\mathcal{L}^* v = \nabla \cdot (\kappa \nabla v) + \mathbf{a} \cdot \nabla v, & \text{USFEM [9].} \end{cases} \tag{6}$$

The methods differ in the treatment of $\nabla \cdot (\kappa \nabla v^h)$ in the added terms.

Definition of the stability parameter τ is discussed in the following sections. We restrict the discussion to linear elements with constant diffusivity within each element. In this case $\nabla \cdot \nabla v^h = 0$ in $\tilde{\Omega}$ and the *three methods coincide*.

3. ONE-DIMENSIONAL ANALYSIS AND DESIGN

We review the analysis of the Galerkin method in one dimension (representing the case of a uniform d-dimensional mesh aligned with a constant velocity) and the design of stability

parameters based on this analysis [5]. The presentation in the following analysis is better suited for generalization to multi-dimensional configurations than the one in [5]. The results and conclusions are identical.

We align the positive x-axis in the direction of the flow. In addition to the constant, an exact, free-space solution to the advection–diffusion equation (1) in one dimension, with constant coefficients and in the absence of sources, is of the form

$$u = \exp(|\mathbf{a}|x/\kappa). \tag{7}$$

3.1. *Spurious Oscillations in the Galerkin Method*

We consider a uniform mesh of linear elements of size h, with nodes at $x_A = Ah$. Nodal values of the exact solution (7) are

$$u(x_A) = (\exp(2\,\alpha))^A, \tag{8}$$

where $\alpha = \frac{|\mathbf{a}|h}{2\kappa}$ is the element Péclet number. Similarly, we assume that corresponding nodal values of finite-element solutions are

$$u_A = (\exp(2\,\alpha^h))^A, \tag{9}$$

where $u_A = u^h\left(x_A\right)$. The dependence of α^h on the element Péclet number α is determined by the analysis of a three-node stencil.

The Galerkin method (3) yields the following equation at interior node A:

$$-(1+\alpha)u_{A-1} + 2\,u_A - (1-\alpha)u_{A+1} = 0. \tag{10}$$

Substituting (9) leads to

$$0 = -(1+\alpha)\exp(-2\alpha^h) + 2 - (1-\alpha)\exp(2\alpha^h) \tag{11}$$

$$= 2 - (\exp(2\,\alpha^h) + \exp(-2\,\alpha^h)) + \alpha(\exp(2\,\alpha^h) - \exp(-2\,\alpha^h)) \tag{12}$$

$$= 2 - 2\cosh(2\alpha^h) + 2\alpha\sinh(2\alpha^h). \tag{13}$$

This simplifies to

$$\sinh(\alpha^h)(\alpha\cosh(\alpha^h) - \sinh(\alpha^h)) = 0. \tag{14}$$

Solutions to this equation are the trivial solution $\alpha^h = 0$ (i.e., the constant is represented exactly) and

$$\alpha^h = \operatorname{arctanh}\alpha. \tag{15}$$

This indicates that α^h approximates α accurately for $\alpha \ll 1$. This presentation may be reconciled with familiar analyses (such as [5]) by noting that

$$\operatorname{arctanh}\alpha = \frac{1}{2}\,\log\frac{1+\alpha}{1-\alpha}, \tag{16}$$

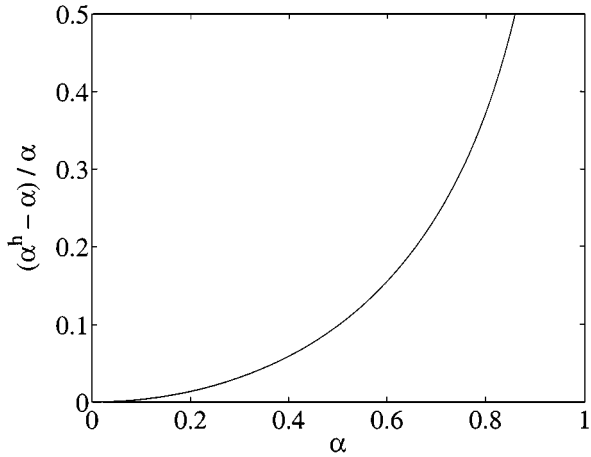

FIG. 1. Error in α^h for Galerkin (3) in the range $\alpha < 1$ ($\alpha^h \in \mathbb{R}$).

so that

$$\exp(2 \operatorname{arctanh} \alpha) = \frac{1+\alpha}{1-\alpha}. \tag{17}$$

According to Eq. (15), α^h is real valued for $\alpha < 1$, approximating α with increasing accuracy as $\alpha \to 0$ (Fig. 1). Considerable degradation in accuracy even prior to the onset of spurious oscillations at $\alpha = 1$ is evident.

For $\alpha > 1$, α^h is complex valued. By relations for hyperbolic functions with complex arguments (see, e.g., [1])

$$\tanh(\alpha^h) = \frac{\sinh(2 \operatorname{Re} \alpha^h) + \mathrm{i} \sin(2 \operatorname{Im} \alpha^h)}{\cosh(2 \operatorname{Re} \alpha^h) + \cos(2 \operatorname{Im} \alpha^h)}. \tag{18}$$

Here $\mathrm{i} = \sqrt{-1}$ is the imaginary unit. We see that

$$\frac{\sin(2 \operatorname{Im} \alpha^h)}{\cosh(2 \operatorname{Re} \alpha^h) + \cos(2 \operatorname{Im} \alpha^h)} = \operatorname{Im} \alpha = 0. \tag{19}$$

Since $\operatorname{Im} \alpha^h \neq 0$, we set

$$\operatorname{Im} \alpha^h = \pi/2. \tag{20}$$

By the Euler formula

$$u_A = (-\exp(2 \operatorname{Re} \alpha^h))^A. \tag{21}$$

The minus sign indicates spurious oscillations. The real part of α^h

$$\operatorname{Re} \alpha^h = \operatorname{arccoth} \alpha, \qquad \alpha > 1 \tag{22}$$

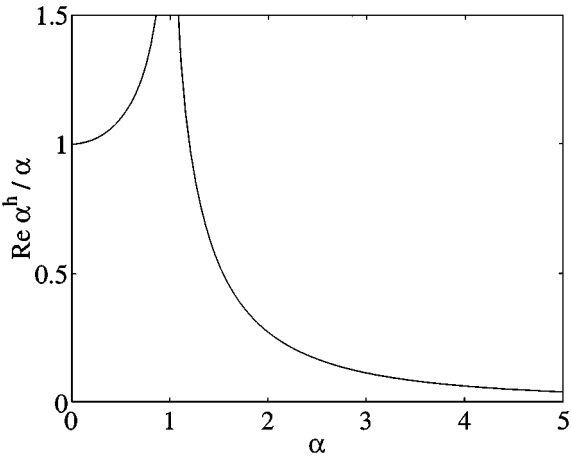

FIG. 2. $\mathrm{Re}\,\alpha^h$ for Galerkin (3) ($\mathrm{Im}\,\alpha^h = \pi/2$ for $\alpha > 1$).

is shown in Fig. 2. In summary

$$\alpha^h = \begin{cases} \operatorname{arctanh}\alpha, & \alpha \le 1 \\ \operatorname{arccoth}\alpha + \mathrm{i}\,\pi/2, & \alpha > 1. \end{cases} \tag{23}$$

3.2. *Stability Parameter*

Repeating the preceding analysis for the stabilized methods (5) (all coincide for linear elements) shows that defining the stability parameter as $\tau = \frac{h}{2|\mathbf{a}|}\,\xi_0$, where

$$\xi_0 = \frac{1}{\tanh\,\alpha} - \frac{1}{\alpha} \tag{24}$$

leads to $\alpha^h = \alpha$.

A different approach to designing the stability parameter is based on bounds from error estimates [9]. For linear elements this results in $\tau = \frac{h}{2|\mathbf{a}|}\,\xi_{\mathrm{FFH}}$, where

$$\xi_{\mathrm{FFH}} = \begin{cases} \alpha/3, & 0 \le \alpha < 3 \\ 1, & 3 \le \alpha. \end{cases} \tag{25}$$

Brooks and Hughes [5] refer to this as a doubly asymptotic approximation (see Fig. 3). Franca *et al.* [9] defined the parameter in terms of the p-norm of **a**. Here we employ the 2-norm. In the following numerical results we refer to this as **FFH.**

Remark. As noted in the Introduction, Galerkin finite elements are related to central differences. In the settings of Section 3.1, the analysis equally applies to central differences, with the same conclusions. The stabilization by the stability parameter of Section 3.2, based on this analysis, is similar in a sense to stabilization by upwind differencing. The important difference between classical upwind differences and stabilized finite elements is in the manner in which the stability parameter is employed, adding stability without yielding accuracy due to the weighted residual form of Eq. (5).

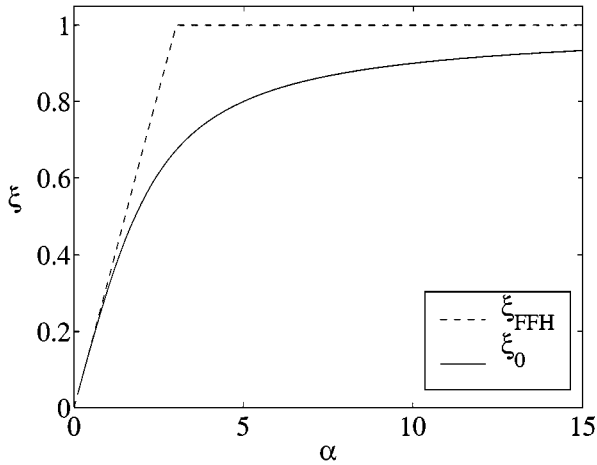

FIG. 3. Different terms in the stability parameter.

4. SPURIOUS ANISOTROPY AND STREAMLINE DESIGN

In addition to the constant, an exact, free-space solution to the multi-dimensional advection–diffusion equation (1), with constant coefficients and in the absence of sources, is of the form

$$u = \exp(\mathbf{a} \cdot \mathbf{x}/\kappa). \tag{26}$$

4.1. *Spurious Anisotropy in the Galerkin Method*

In contrast to exact solutions, Galerkin solutions are anisotropic in the sense that they depend on the orientation of the mesh with respect to the given velocity. This phenomenon is demonstrated in the following analysis.

We consider a uniform, two-dimensional mesh of bilinear elements of size h, aligned with the global axes, with nodes at $\mathbf{x}_A = (mh, nh)$. Since $\mathbf{a}^T = |\mathbf{a}|\langle \cos\theta, \sin\theta \rangle$, nodal values of the exact solution (26) are

$$u(\mathbf{x}_A) = (\exp(2\,\alpha c))^m (\exp(2\,\alpha s))^n, \tag{27}$$

where $c = \cos\theta$ and $s = \sin\theta$. Similarly, we assume that corresponding nodal values of finite-element solutions are

$$u_A = (\exp(2\,\alpha^h c))^m (\exp(2\,\alpha^h s))^n, \tag{28}$$

where $u_A = u^h(\mathbf{x}_A)$. The dependence of α^h on the element Péclet number α and the orientation of the mesh with respect to the streamline direction is determined by the analysis of a nine-node patch (Fig. 4).

The Galerkin method (3) yields the following equation at interior node A:

$$\begin{aligned} &\sinh(\alpha^h c)(\alpha c \cosh(\alpha^h c) - \sinh(\alpha^h c))(3 + 2\,\sinh^2(\alpha^h s)) \\ &\quad + \sinh(\alpha^h s)(\alpha s \cosh(\alpha^h s) - \sinh(\alpha^h s))(3 + 2\,\sinh^2(\alpha^h c)) = 0. \end{aligned} \tag{29}$$

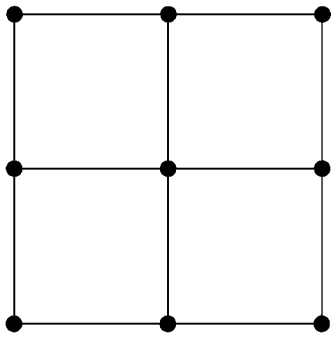

FIG. 4. Nine-node patch.

The trivial solution $\alpha^h = 0$ satisfies this equation (i.e., the constant is represented exactly). There is an additional solution, corresponding to Eq. (15) when the mesh is aligned with the flow. The variation of this solution with the orientation of the mesh with respect to the streamline direction (θ) is shown in Fig. 5, for cases in which α^h is real valued ($\alpha < 1$). Note that the best performance is attained when the flow is along element diagonals ($\theta = \pi/4$).

4.2. *Streamline Design of the Stability Parameter*

Repeating the preceding analysis for the stabilized methods (5) (all coincide for the mesh considered) provides an optimal definition of the stability parameter

$$\tau = \frac{h}{2|\mathbf{a}|}\,\frac{1}{\alpha}\,\frac{tc(c\alpha - tc)(3/cs^2 + 2ts^2) + ts(s\alpha - ts)(3/cc^2 + 2tc^2)}{3c^2(tc/cs)^2 + 3s^2(ts/cc)^2 + 2tc^2ts^2 + 6cs\ tc\ ts} \tag{30}$$

that leads to $\alpha^h = \alpha$ for any orientation. Here $cc = \cosh(c\alpha)$, $cs = \cosh(s\alpha)$, $tc = \tanh(c\alpha)$, and $ts = \tanh(s\alpha)$. This form of the definition is chosen to reduce sensitivity to finite arithmetic.

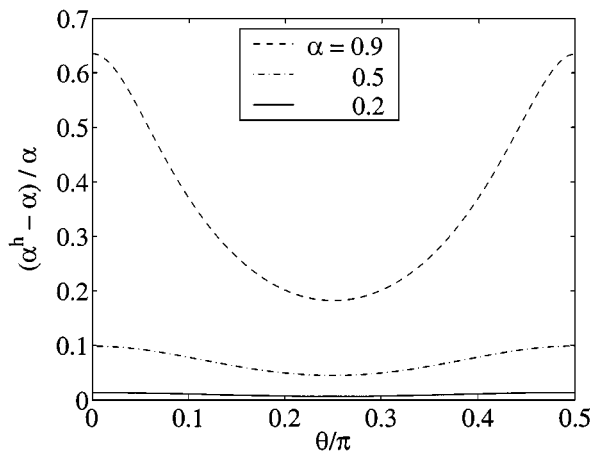

FIG. 5. Anisotropy in Galerkin method.

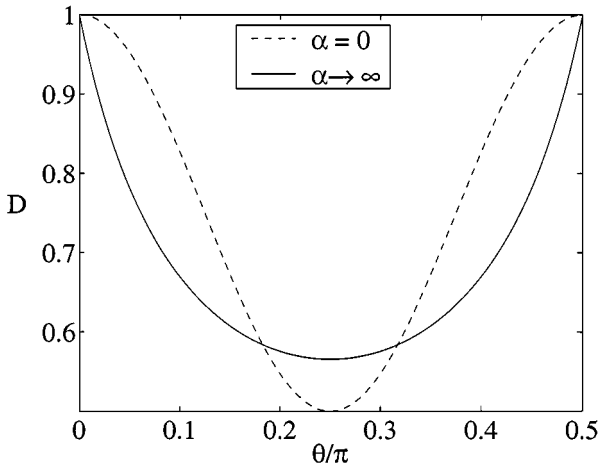

FIG. 6. Directivity in both limits.

In the limits, this streamline parameter may be expressed simply as

$$\tau = \frac{h}{2|\mathbf{a}|}\, D(\theta)\, \xi_0(\alpha), \tag{31}$$

where

$$D = \begin{cases} c^4 + s^4, & \alpha = 0, \\ \frac{c+s}{1+3cs} \quad (0 \le \theta \le \pi/2), & \alpha \to \infty. \end{cases} \tag{32}$$

The least amount of stabilization is applied when the flow is along element diagonals ($\theta = \pi/4$, Fig. 6), i.e., when the performance of Galerkin is at its best (Fig. 5).

The difference between the two cases of D is not large. This suggests a definition of the parameter that may be employed in practice. Since the advection-dominated case ($\alpha \gg 1$) is the challenging regime, we propose

$$\tau = \frac{h}{2|\mathbf{a}|}\, \frac{\cos\theta + \sin\theta}{1 + 3\,\cos\theta\,\sin\theta} \left(\frac{1}{\tanh\alpha} - \frac{1}{\alpha} \right). \tag{33}$$

Note that the orientation should be regarded so that $0 \le \theta \le \pi/2$. This presents no practical limitation.

In the following numerical results we refer to the parameter that leads to $\alpha^h = \alpha$, defined by Eq. (30) as the streamline parameter (**STR**), and the one defined by Eq. (33) is called the estimated parameter (**EST**).

5. NUMERICAL RESULTS

In this section we compare the numerical performance of stabilized finite-element methods with the proposed parameters to established techniques. We consider the following methods:

STR Stabilized finite elements with the streamline parameter (30).

EST Stabilized finite elements with the estimated streamline parameter (33).

FFH Stabilized finite elements with the FFH parameter [9], see (25).

RFB The method of residual-free bubbles, with the bubble derived for the advective limit [3].

We use bilinear elements in all tests.

5.1. *Smooth Boundary Layer*

Consider a constant-coefficient advective–diffusive problem in the unit square $]0, 1[\times]0, 1[$. There are no distributed sources ($f = 0$). Inhomogeneous Dirichlet data are specified on the boundaries so that the solution is

$$u(\mathbf{x}) = \frac{\exp((\mathbf{x} - \mathbf{x}_c) \cdot \mathbf{a}\,/\kappa) - 1}{\exp(-\mathbf{x}_c \cdot \mathbf{a}\,/\kappa) - 1}, \tag{34}$$

where $\mathbf{x}_c = (1, 1)$. The solution is of the form of (26), normalized so that $0 \le u \le 1$. We use a uniform mesh with 20×20 elements. Table I shows the relative error, measured in the L_2 norm. The error relative to the exact solution at $\theta = 0$ is consistently larger since the boundary layer spreads along an entire side of the domain, whereas in other cases it is concentrated in a corner. In all cases, the interpolation error dominates. For **STR** and **EST** the approximation error is negligible. The **EST** results are comparable to **STR**, so from here on we show only **EST** results.

5.2. *Advection Skew to the Mesh*

We modify Problem 5.1 so that there is a discontinuity in the inflow Dirichlet data at $\mathbf{x} = (0.475, 0)$, with homogeneous Neumann outflow conditions (Fig. 7). The discontinuity is propagated into the domain creating an internal layer. Here $\alpha = 2.5 \times 10^4$. A piecewise constant reference solution (based on the advective limit) is set equal to the inhomogeneous Dirichlet value to the left of the discontinuity, and zero to the right. The problem is solved at $\theta = \pi/6, \pi/4$, and $\pi/3$. For example, solutions at $\theta = \pi/3$ are shown in Fig. 8. **EST** provides some improvement over **FFH**, yet **RFB** exhibits the best performance for these problems with discontinuities, particularly when the flow is along element diagonals (Fig. 9).

TABLE I
L_2 Relative Errors [%], Problem 5.1

		Relative to exact solution			Relative to nodal interpolant		
α	θ/π	**STR**	**EST**	**FFH**	**STR**	**EST**	**FFH**
2.5	0	7.62	7.62	8.59	4.51×10^{-14}	5.25×10^{-14}	1.81
	1/6	1.14	1.15	1.25	5.04×10^{-14}	3.28×10^{-2}	0.337
	1/4	1.14	1.15	1.26	5.58×10^{-14}	4.74×10^{-2}	0.362
250	0	12.8	12.8	12.9	1.13×10^{-13}	9.75×10^{-14}	3.65×10^{-2}
	1/6	1.67	1.67	1.75	5.22×10^{-14}	1.27×10^{-3}	0.361
	1/4	1.67	1.67	1.77	6.17×10^{-14}	1.20×10^{-3}	0.411
2.5×10^4	0	12.9	12.9	12.9	9.87×10^{-14}	1.00×10^{-13}	3.66×10^{-4}
	1/6	1.67	1.67	1.75	7.31×10^{-14}	1.28×10^{-5}	0.361
	1/4	1.67	1.67	1.77	6.12×10^{-14}	1.21×10^{-5}	0.410

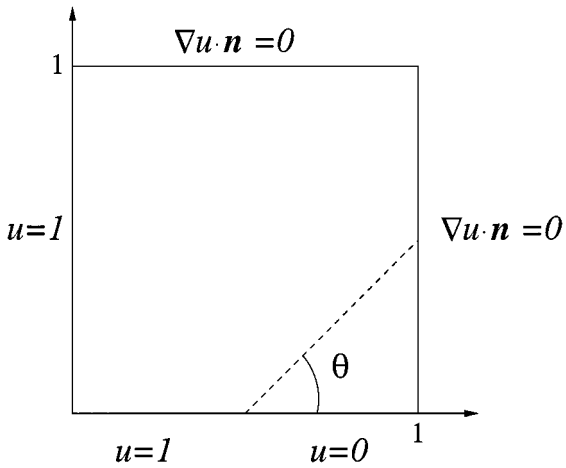

FIG. 7. Statement of Problem 5.2.

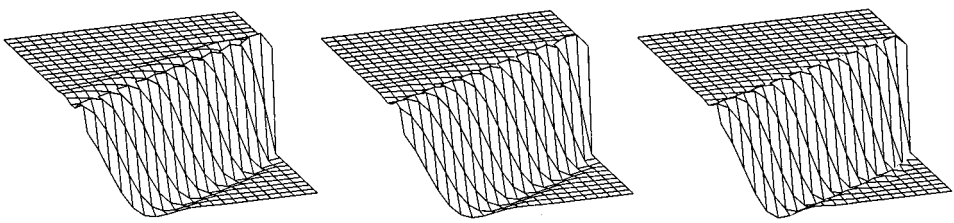

FIG. 8. Solutions of Problem 5.2 at $\theta = \pi/3$: **EST** (left), **FFH** (center), and **RFB** (right).

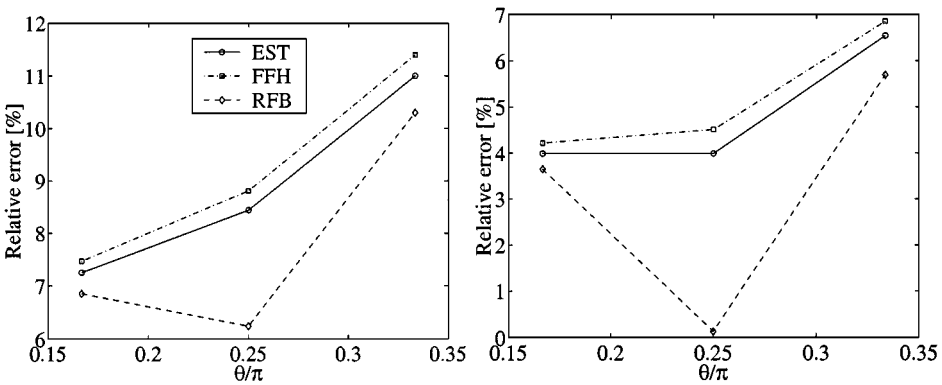

FIG. 9. L_2 error [%] in Problem 5.2 relative to reference solution (left) and nodal interpolant (right).

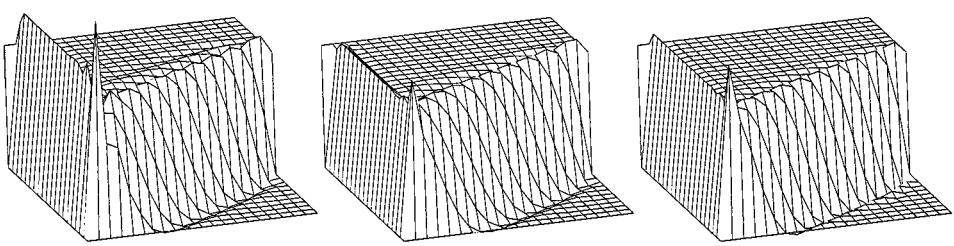

FIG. 10. Solutions of Problem 5.3 at $\theta = \pi/3$: **EST** (left), **FFH** (center), and **RFB** (right).

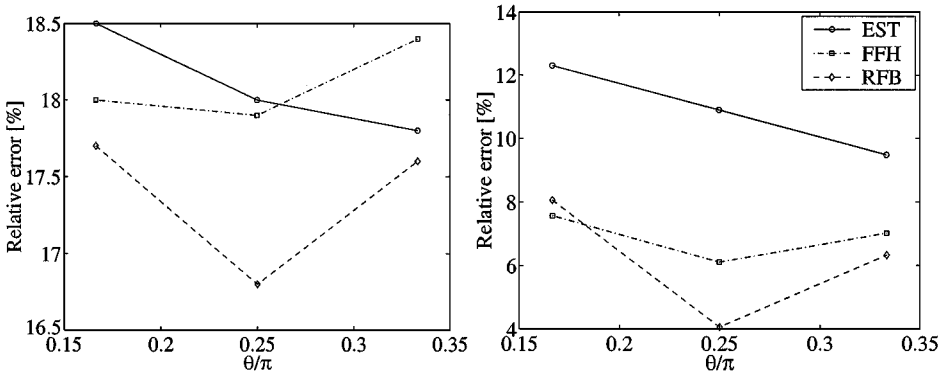

FIG. 11. L_2 error [%] in Problem 5.3 relative to reference solution (left) and nodal interpolant (right).

5.3. *Advection Skew to the Mesh with Outflow Boundary Layers*

The outflow conditions of Problem 5.2 are changed to homogeneous Dirichlet conditions, leading to outflow boundary layers [3, 9]. The reference solution is unchanged in the domain, but the interpolant now accounts for the outflow boundary layers. The problem is solved at $\theta = \pi/6, \pi/4$, and $\pi/3$. For example, solutions at $\theta = \pi/3$ are shown in Fig. 10. Figure 11 shows the relative error. The outflow boundary layers are numerically challenging, but may not represent typical physical configurations. The **EST** parameter is designed to reduce stabilization based on the streamline direction (see Fig. 6), which is inappropriate for the outflow boundary layers in this problem, leading to the relative deterioration in the **EST** results (Fig. 11).

5.4. *Transport in a Rotating Flow Field*

Consider a homogeneous Dirichlet advective–diffusive problem [9, 15] in the unit square (centered at the origin, Fig. 12). There are no distributed sources ($f = 0$), $\kappa = 10^{-6}$, and $\mathbf{a}^T = \langle -y, x \rangle$, representing a rotating velocity field. There is an internal boundary along

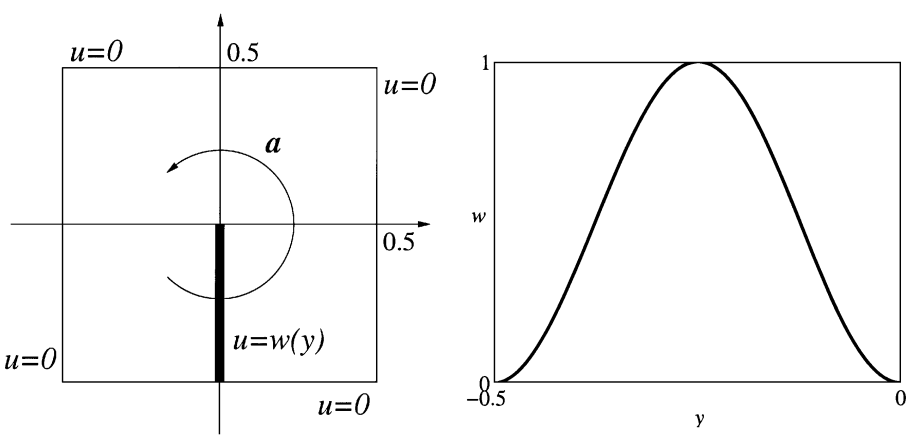

FIG. 12. Statement of Problem 5.4.

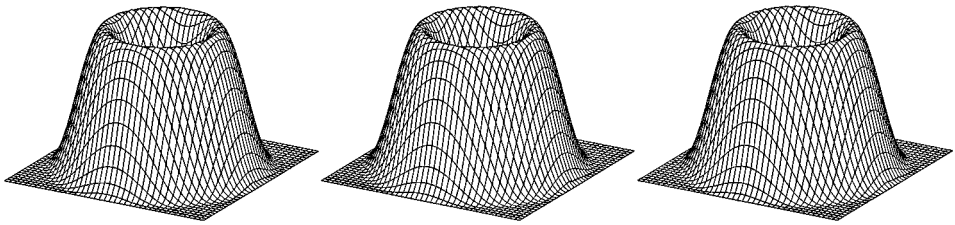

FIG. 13. Solutions of Problem 5.4: **EST** (left), **FFH** (center), and **RFB** (right).

the negative y-axis, with the boundary condition $u(0, y) = w(y)$, where

$$w(y) = \frac{1}{2}[\cos(4\pi y + \pi) + 1], \qquad -0.5 \le y \le 0. \tag{35}$$

The reference solution is obtained by **FFH** on a uniform mesh of 200×200 elements. The tests are performed on a uniform mesh of 40×40 elements. Stability parameters are evaluated in terms of velocity at element centers. Solutions are shown in Fig. 13. Table II shows the relative error, measured in the L_2 norm. **EST** exhibits the best performance on this smooth problem. We note that the version of **RFB** implemented herein is designed for the advective limit, while this problem contains diffusion-dominated regions.

5.5. *Transport in Flow Over a Backwards Facing Step*

Consider the transport problem outlined in Fig. 14, with $\kappa = 10^{-6}$ and no distributed sources ($f = 0$).

The background flow is governed by the steady-state, incompressible Navier–Stokes equations, with Dirichlet boundary conditions as shown in Fig. 15. Parabolic patterns are specified at both inflow and outflow boundaries. The maximum inflow velocity is of unit magnitude, leading to a Reynolds number $\mathrm{Re} = 60$ with respect to the width of the inflow region. The magnitude of the outflow velocity is determined by incompressibility (accounting for interpolation of the parabolic distributions by piecewise finite-element polynomials); see, e.g., [13, p. 193].

The background flow is calculated by a stabilized finite-element method for the incompressible Navier–Stokes equations [8] on a uniform mesh with bilinear, square elements of side $h = 1/512$. Figure 16 shows the resulting vector field. This flow is used as input to the advective–diffusive transport problem.

The reference solution to the transport problem is obtained by **FFH** on the same mesh used to compute the background flow ($h = 1/512$). Tests are performed on uniform meshes with square elements of side h, where $h = 1/32$, $1/64$, $1/128$, and $1/256$. Stability parameters are evaluated in terms of velocity at element centers. Accurate integration is employed to account for the rapid variation of the background flow in some regions. Representative solutions are shown in Figs. 17 and 18.

Figure 19 shows the relative error, measured in the L_2 norm. The version of **RFB** implemented herein is designed for the advective limit, while this problem contains diffusion-dominated regions. Nonetheless, **RFB** exhibits the best performance except on the finest mesh. (More regions are "numerically" diffusion-dominated as the mesh is refined.) **EST** exhibits a small improvement over **FFH** on all meshes.

TABLE II
L_2 Relative Errors [%], Problem 5.4

	Relative to reference solution	Relative to nodal interpolation
EST	0.779	0.344
FFH	0.904	0.484
RFB	0.809	0.353

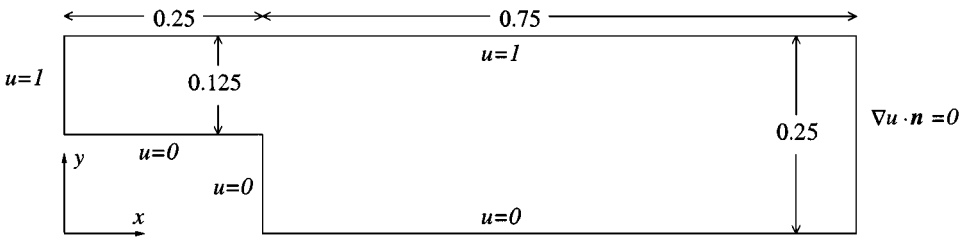

FIG. 14. Statement of Problem 5.5.

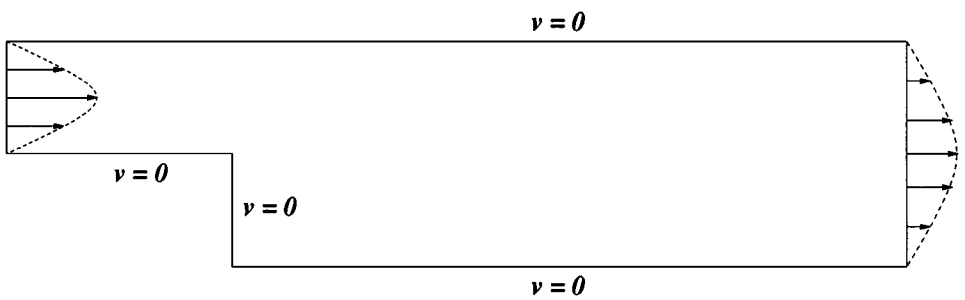

FIG. 15. Statement of background flow problem for Problem 5.5.

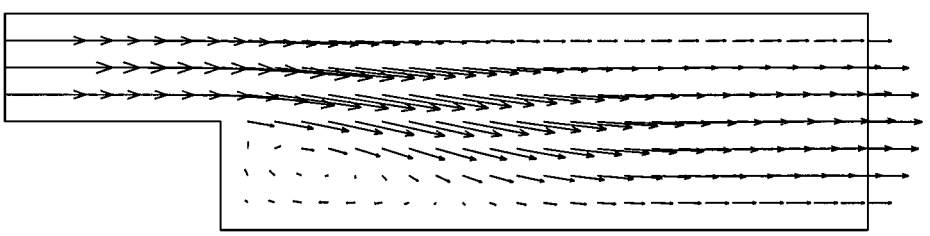

FIG. 16. Computed background flow field for Problem 5.5.

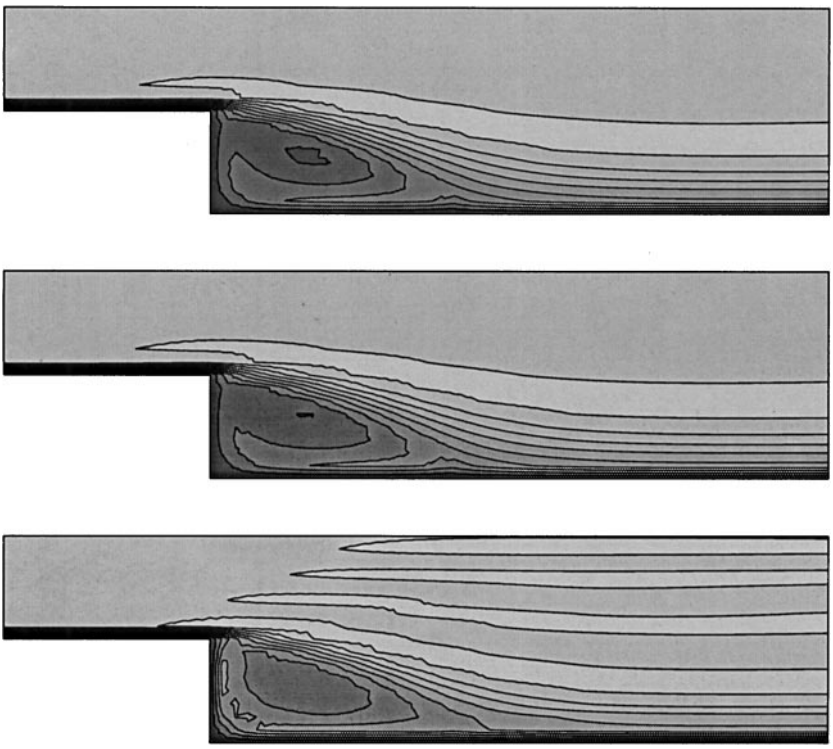

FIG. 17. Solutions of Problem 5.5 at $h = 1/64$: **EST** (top), **FFH** (center), and **RFB** (bottom).

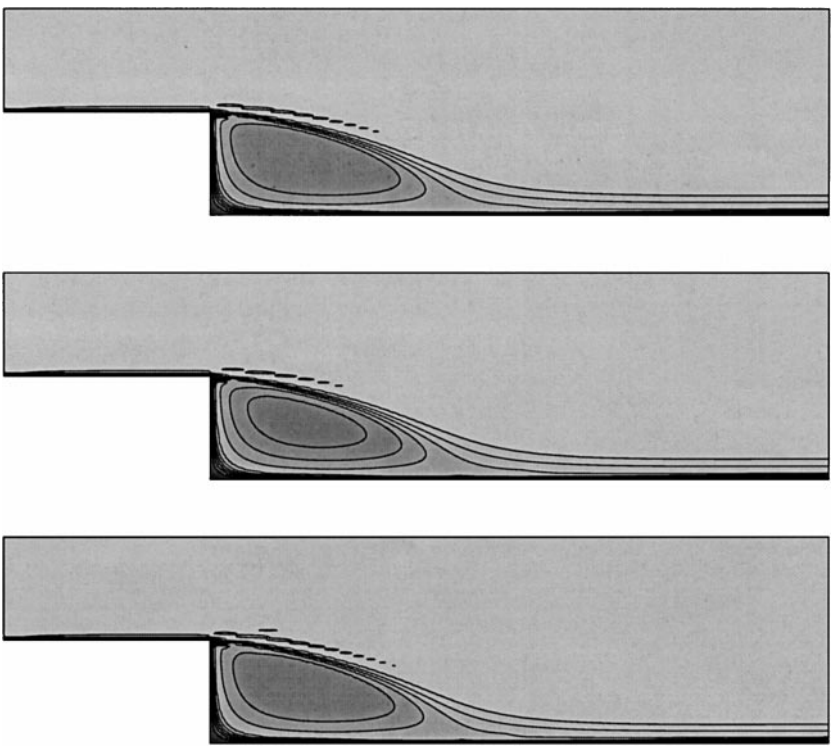

FIG. 18. Solutions of Problem 5.5 at $h = 1/256$: **EST** (top), **FFH** (center), and **RFB** (bottom).

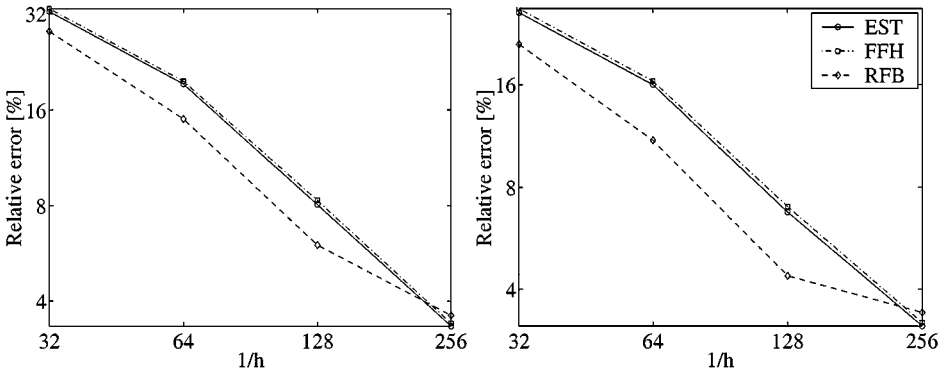

FIG. 19. L_2 error [%] in Problem 5.5 relative to reference solution (left) and nodal interpolant (right).

6. CONCLUSIONS

The classical Galerkin finite-element method performs poorly in the computation of convection-dominated transport phenomena, even prior to the onset of spurious oscillations. This deficiency may be alleviated by stabilization. A family of stabilized methods has evolved over the last two decades, including Galerkin/least-squares, SUPG (also known as streamline diffusion), and the unusual stabilized finite element method. These three methods share the approach of appending to the Galerkin equation terms containing residual-based operators multiplied by stabilization parameters. The residual-based operators naturally account for the direction of the flow. The stability parameter is typically designed on the basis of model problems or bounds from error analyses. Heretofore the flow direction has been ignored or regarded on an *ad hoc* basis.

In this work we analyze the spurious anisotropy inherent in the Galerkin method, i.e., the dependence of the solution on the orientation of the mesh with respect to the flow direction. On the basis of this analysis we propose definitions of the stability parameter that rationally incorporate the flow direction. One particularly simple and economical definition (33) is recommended for practical application. Numerical tests compare the performance of the proposed method with established techniques. Employing the simple parameter that accounts for the flow direction generally improves the performance of the stabilized methods.

REFERENCES

1. M. Abramowitz and I. A. Stegun, editors, *Handbook of Mathematical Functions with Formulas, Graphs, and Mathematical Tables*, Number 55 in Applied Mathematics Series (U.S. Department of Commerce, National Bureau of Standards, Washington, D.C., 1972).
2. F. Brezzi, M. O. Bristeau, L. P. Franca, M. Mallet, and G. Rogé, A relationship between stabilized finite element methods and the Galerkin method with bubble functions, *Comput. Methods Appl. Mech. Eng.* **96**(1), 117 (1992).
3. F. Brezzi, L. P. Franca, and A. Russo, Further considerations on residual-free bubbles for advective–diffusive equations, *Comput. Methods Appl. Mech. Eng.* **166**(1–2), 25 (1998).
4. F. Brezzi and A. Russo, Choosing bubbles for advection–diffusion problems, *Math. Models Methods Appl. Sci.* **4**(4), 571 (1994).

5. A. N. Brooks and T. J. R. Hughes, Streamline upwind/Petrov–Galerkin formulations for convection dominated flows with particular emphasis on the incompressible Navier–Stokes equations, *Comput. Methods Appl. Mech. Eng.* **32**(1–3), 199 (1982). FENOMECH '81, Part I (Stuttgart, 1981).
6. L. P. Franca and C. Farhat, Bubble functions prompt unusual stabilized finite element methods, *Comput. Methods Appl. Mech. Eng.* **123**(1–4), 299 (1995).
7. L. P. Franca, C. Farhat, A. P. Macedo, and M. Lesoinne, Residual-free bubbles for the Helmholtz equation, *Int. J. Numer. Meth. Eng.* **40**(21), 4003 (1997).
8. L. P. Franca and S. L. Frey, Stabilized finite element methods. II. The incompressible Navier–Stokes equations, *Comput. Methods Appl. Mech. Eng.* **99**(2–3), 209 (1992).
9. L. P. Franca, S. L. Frey, and T. J. R. Hughes, Stabilized finite element methods. I. Application to the advective-diffusive model, *Comput. Methods Appl. Mech. Eng.* **95**(2), 253 (1992).
10. L. P. Franca and A. P. Macedo, A two-level finite element method and its application to the Helmholtz equation, *Int. J. Numer. Methods Eng.* **43**(1), 23 (1998).
11. L. P. Franca, A. Nesliturk, and M. Stynes, On the stability of residual-free bubbles for convection–diffusion problems and their approximation by a two-level finite element method, *Comput. Methods Appl. Mech. Eng.* **166**(1–2), 35 (1998).
12. L. P. Franca and F. Valentin, On an improved unusual stabilized finite element method for the advective–reactive–diffusive equation, *Comput. Methods Appl. Mech. Eng.* **189**(13–14), 1785 (2000).
13. T. J. R. Hughes, *The Finite Element Method* (Prentice-Hall, Englewood Cliffs, NJ, 1987).
14. T. J. R. Hughes, Recent progress in the development and understanding of SUPG methods with special reference to the compressible Euler and Navier–Stokes equations, *Int. J. Numer. Methods Fluids* **7**(11), 1261 (1987).
15. T. J. R. Hughes and A. Brooks, A multi-dimensional upwind scheme with no crosswind diffusion, in *Finite Element Methods for Convection Dominated Flows*, AMD, edited by T. J. R. Hughes (ASME, New York, 1979), Vol. 34, pp. 19–35.
16. T. J. R. Hughes, L. P. Franca, and G. M. Hulbert, A new finite element formulation for computational fluid dynamics. VIII. The Galerkin/least-squares method for advective–diffusive equations, *Comput. Methods Appl. Mech. Eng.* **73**(2), 173 (1989).
17. G. D. Raithby, Skew upstream differencing schemes for problems involving fluid flow, *Comput. Methods Appl. Mech. Eng.* **9**(2), 153 (1976).
18. P. J. Roache, *Computational Fluid Dynamics* (Hermosa Publishers, Albuquerque, NM, 1976). With an appendix ("On artificial viscosity") reprinted from *J. Comput. Phys.* **10**(2), 169 (1972), revised printing.
19. L. B. Wahlbin, A dissipative Galerkin method for the numerical solution of first order hyperbolic equations, *Mathematical Aspects of Finite Elements in Partial Differential Equations, Proc. Sympos., Math. Res. Center, Univ. Wisconsin, Madison, Wis., 1947* (Math. Res. Center, Univ. of Wisconsin-Madison, Academic Press, New York 1974), Publication No. 33, pp. 147–169.